Heliyon 10 (2024) e28152

Contents lists available at ScienceDirect

Heliyon

journal homepage: www.cell.com/heliyon

Research article

Spatio-temporal evaluation of air pollution using ground-based and satellite data during COVID-19 in Ecuador

Danilo Mejía C [a,b,*], Gina Faican [a], Rasa Zalakeviciute [c], Carlos Matovelle [d], Santiago Bonilla [e], José A. Sobrino [f]

[a] Grupo CATOx – CEA de la Universidad de Cuenca, Campus Balzay, 010207 Cuenca, Ecuador
[b] Carrera de Ingeniería Ambiental de la Universidad de Cuenca, Campus Balzay, 010207 Cuenca, Ecuador
[c] Grupo de Biodiversidad Medio Ambiente y Salud (BIOMAS), Universidad de Las Americas, Quito - EC 170125, Ecuador
[d] Carrera de Ingeniería Ambienta de la Universidad Católica de Cuenca, Ecuador
[e] Research Center for the Territory and Sustainable Habitat, Universidad Tecnológica Indoamérica, Machala y Sabanilla, 170301 Quito, Ecuador
[f] Gobal Change Unit (GCU), Image Processing Laboratory (IPL), University of Valencia, Spain

ARTICLE INFO

Keywords:
Sentinel-5P
NO_2
O_3
COVID-19
Atmospheric pollution
linear regression model

ABSTRACT

The concentration of gases in the atmosphere is a topic of growing concern due to its effects on health, ecosystems etc. Its monitoring is commonly carried out through ground stations which offer high precision and temporal resolution. However, in countries with few stations, such as Ecuador, these data fail to adequately describe the spatial variability of pollutant concentrations. Remote sensing data have great potential to solve this complication. This study evaluates the spatiotemporal distribution of nitrogen dioxide (NO_2) and ozone (O_3) concentrations in Quito and Cuenca, using data obtained from ground-based and Sentinel-5 Precursor mission sources during the years 2019 and 2020. Moreover, a Linear Regression Model (LRM) was employed to analyze the correlation between ground-based and satellite datasets, revealing positive associations for O_3 ($R^2 = 0.83$, RMSE = 0.18) and NO_2 ($R^2 = 0.83$, RMSE = 0.25) in Quito; and O_3 ($R^2 = 0.74$, RMSE = 0.23) and NO_2, ($R^2 = 0.73$, RMSE = 0.23) for Cuenca. The agreement between ground-based and satellite datasets was analyzed by employing the intra-class correlation coefficient (ICC), reflecting good agreement between them (ICC $\geq$0.57); and using Bland and Altman coefficients, which showed low bias and that more than 95% of the differences are within the limits of agreement. Furthermore, the study investigated the impact of COVID-19 pandemic-related restrictions, such as social distancing and isolation, on atmospheric conditions. This was categorized into three periods for 2019 and 2020: before (from January 1st to March 15th), during (from March 16th to May 17th), and after (from March 18th to December 31st). A 51% decrease in NO_2 concentrations was recorded for Cuenca, while Quito experienced a 14.7% decrease. The tropospheric column decreased by 27.3% in Cuenca and 15.1% in Quito. O_3 showed an increasing trend, with tropospheric concentrations rising by 0.42% and 0.11% for Cuenca and Quito respectively, while the concentration in Cuenca decreased by 14.4%. Quito experienced an increase of 10.5%. Finally, the reduction of chemical species in the atmosphere as a consequence of mobility restrictions is highlighted. This study compared satellite and ground station data for NO_2 and O_3 concentrations. Despite differing units preventing data validation, it verified the Sentinel-5P satellite's effectiveness in anomaly detection. Our research's value lies in its applicability to

* Corresponding author. Grupo CATOx – CEA de la Universidad de Cuenca, Campus Balzay, 010207 Cuenca, Ecuador.
E-mail addresses: danilo.mejia@ucuenca.edu.ec (D. Mejía C), gifaican@gmail.com (G. Faican), rasa.zalake@gmail.com (R. Zalakeviciute), cmmatovelleb@ucacue.edu.ec (C. Matovelle), santiagobonilla@uti.edu.ec (S. Bonilla), Jose.Sobrino@uv.es (J.A. Sobrino).

https://doi.org/10.1016/j.heliyon.2024.e28152
Received 3 June 2023; Received in revised form 27 February 2024; Accepted 13 March 2024
Available online 20 March 2024

developing countries, which may lack extensive monitoring networks, demonstrating the potential use of satellite technology in urban planning.

1. Introduction

Air pollution has become the greatest challenge to global public health; its impacts also threaten the integrity of ecosystems, and material goods, and alter the climate [1–4]. In particular, developing countries face significant pollution problems, leading to air quality levels below those recommended by the World Health Organization (WHO), thus imposing economic and health burdens on the inhabitants of these regions [5,6].

The primary air pollutants include carbon monoxide (CO), sulfur dioxide (SO_2), nitrogen monoxide and nitrogen dioxide (NO and NO_2), ozone (O_3), and particulate matter with aerodynamic diameters less than 10 (PM_{10}) and 2.5 ($PM_{2.5}$) microns. These pollutants are primarily emitted by transportation, industries, agricultural production, and waste generation [7]. NO_2 and O_3 are severe and harmful pollutants, with NO_2 causing respiratory illnesses and even cognitive implications [7–9]. Their concentrations are strongly linked to human activity, mainly due to the burning of fuels caused by vehicular traffic and industrial activities [10]. Moreover, NO_2 is a crucial precursor to tropospheric O_3 [11], which, due to its highly oxidizing nature, can have acute and chronic effects on pulmonary and cardiovascular morbidity, and even cause premature mortality [12,13].

Despite efforts to control the sources of atmospheric pollutant emissions, our country's economic growth dynamics are strongly linked to the transportation and industrial sectors [14], making it unfeasible to restrict these origins. On the other hand, the COVID-19 pandemic led to extraordinary restrictive measures to curb the spread of the virus. Social distancing and isolation were progressively implemented in Ecuador starting on March 17, 2020, improving air quality [15]. For this study, March, April and May are established as period of special interest, because they were the months with the greatest restriction.

Various studies around the world have demonstrated a decrease in pollution as a result of restrictive measures and/or lockdowns, mainly in NO_2 [16–19], whose decrease resulted in an increase in O_3 concentrations; phenomenon documented previously and with current studies highlights the complex interconnection between these components of the atmosphere [20–26]. The variability in concentrations was more noticeable in cities with higher population densities than those with lower population densities.

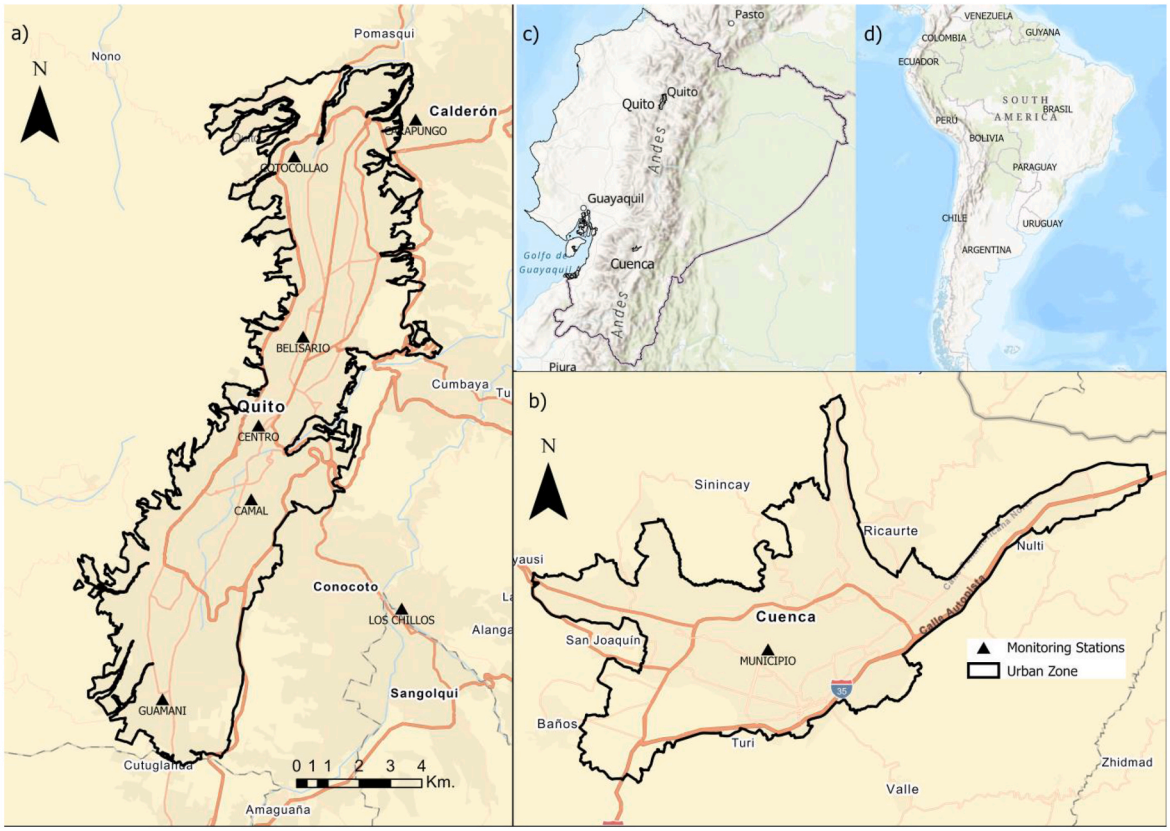

Fig. 1. Map indicating the study area's location: a) Quito, situated in northern Ecuador; b) Cuenca, located in southern Ecuador; c) study sites throughout Ecuador; and d) Ecuador's position within South America.

This study has evaluated this phenomenon in Quito and Cuenca, which account for approximately 18.6% of Ecuador's total population, a large part of the automobile fleet, and essential industries located within their boundaries. Both areas are equipped with air quality monitoring networks that collect, process, and disseminate real-time information regarding surface concentrations on an urban scale, covering a range of up to 50 km [27].

Therefore, it is vital to identify methodologies that allow us to make accurate inferences about air quality variability. Mejía C. et al. [27], Arikan & Yildiz [28], and Zalakeviciute et al. [29] have relied on information derived from Sentinel-5 Precursor satellite data carried by the TROPOspheric Monitoring Instrument (TROPOMI) to monitor pollutant concentrations. Satellite detection is also limited regarding the actual transport and transformation of pollutants by the presence of clouds, which affect continuous and uniform sampling and coverage [10].

As mentioned above, the historical drops in atmospheric pollutant levels during the COVID-19 pandemic are an ideal scenario to evaluate the performance of atmospheric pollutant measurement methodologies, mainly satellite remote sensing. This research aims to evaluate the temporal behavior of NO_2 and O_3 concentrations in the atmosphere during the years 2019 and 2020, through surface and Sentinel-5P derived data in the cities of Quito and Cuenca, Ecuador. In addition, the impact of restrictive measures in the country on pollutant emissions has been quantified by calculating the rate of change recorded by the two data sets.

2. Methods

2.1. Study area

The study area corresponds to Quito and Cuenca, located in Ecuador (Fig. 1c and d), some of the most representative cities in the country at a demographic and industrial level. They are also the only two cities that manage air quality in Ecuador through permanent monitoring networks, allowing air quality trends to be established based on data reliable and continuous. Quito (Fig. 1a) is located in the central northern area of the country at Latitude 0° 13′ 07″ S and Longitude 77°30′35″ W. Its territory spans around 372.4 km^2 of irregular topography with 44 climatic zones and ecosystems; it displays a significant altitudinal variation with elevations ranging from 1200 m above sea level (m.a.s.l.) in the northwest to 4794 m.a.s.l. at the Pichincha volcano massif located to the west [30]. Its approximate population is 2.011 million inhabitants, of which 68.7% reside in the urban area.

Cuenca is located within the canton of the same name in the south-central zone of the country (Fig. 1b), it has an area of 73 km^2, its altitudes vary between 2560 and 3100 m.a.s.l [31,32]. In 2018 it registered an estimated population of 614539 inhabitants, of which 65.64% belonged to the urban area [33]. Both cities are located in the inter-Andean alley of the Andes Mountains and according to the Köppen-Geiger classification their climate corresponds to Cfb (marine west coast), characteristic of mid-latitudes, humid and temperate [31,34].

In the city of Cuenca, NO_2 and O_3 data are collected by a single station, located in the city's center. In Quito, data are collected by eight stations distributed mainly in the urban area, except for three (Carapungo, Tumbaco and Los Chillos) located in rural areas. Table 1 shows the characteristics of the stations mentioned above.

2.2. Ground-based data

The data correspond to the information provided by ground-based stations. One station is located in Cuenca on top of the Municipal Building (MUN), and there are eight stations in Quito: Belisario, Camal, Carapungo, Centro, Los Chillos, Cotocollao, Guamaní, and Tumbaco. These stations are distributed across different points within the canton and at varying elevations (Fig. 1 and Table 1). The temporal coverage of data for O_3 is 94.08% in Quito and 98.6% in Cuenca, and for NO_2, it is 93.70% in Quito and 97.8% in Cuenca [35, 36], covering the dates from January 01, 2019 to December 31, 2020.

The stations have urban-neighborhood coverage (4–50 km) and a sampling rate of one per minute (real-time), from which the means are calculated in the periods established in the NCAA (daily for NO_2 and eight-hourly for O_3). The recording methodologies and instrumentation used are listed in Table 2.

For data dissemination, the data are available at an hourly frequency, reported in μg m^{-3}, and are freely accessible through the digital platforms of Quito's Environment Secretariat (http://datosambiente.quito.gob.ec/) and the Municipal Public Company of Mobility, Transit and Transportation of Cuenca (EMOV EP) in Cuenca (http://caire.emov.gob.ec/monitoreo/pages/get-data.xhtml?

Table 1
Surface monitoring stations.

Code	City-Area	Name	Latitud	Longitud	Altitude
MUN	Cuenca - Centro Histórico	Municipio	2°53′50″ S	79°00′14″ W	2538
BEL	Quito – Norte	Belisario	0°10′48″ S	78°29′24″ W	2835
CAR	Quito – Calderón	Carapungo	0°5′54″ S	78°26′50″ W	2851
CAM	Quito – Sur	Camal	0°15′00″ S	78°30′36″ W	2840
CEN	Quito – Centro	Centro	0°13′12″ S	78°30′36″ W	2820
LCH	Quito - Los Chillos	Los Chillos	0°18′00″ S	78°27′36″ W	2453
COT	Quito - La Delicia	Cotocollao	0°6′28″ S	78°29′50″ W	2739
GUA	Quito – Quitumbe	Guamaní	0°19′51″ S	78°33′50″ W	3066
TUM	Quito – Tumbaco	Tumbaco	0°12′36″ S	78°24′00″ W	2331

Table 2
Characteristics of ground-based instruments.

Gas	Place	Recovery methodology	Instrument	Equivalent Method
O_3	Quito	UV radiation absorption	Thermo 49C/49i	USEPA No. EQOA-0880-047
	Cuenca		Teledyne M400E	USEPA EQOA-0992-087
NO_2	Quito	Chemiluminescence	Thermo 42C/42i	USEPA No. RFNA-1289-074
	Cuenca		Teledyne M200E	USEPA RFNA-1194-099

dataType=AIR&avgType=DAYLI).

The hourly ground-based data were processed to obtain the monthly mean per gas during the specified period, generating a database with 24 records per station and pollutant.

2.3. Satellite data

NO_2 and O_3 concentrations in μmol m^{-2} columns were obtained from the TROPOMI instrument on board the Sentinel-5P. For our analysis, we used L3 level satellite data of monthly means with a spatial resolution of 1 km^2, provided by the Google Earth Engine (GGE) platform (https://earthengine.google.com/). The data correspond to monthly means from January 01, 2019 to December 31, 2020 concentrations for NO_2 and O_3. However, the spatial visualization of pollutants was categorized into three periods for the years 2019 and 2020: before (from January 1st to March 15th), during (from March 16th to May 17th), and after (from May 18th to December 31st) (Table 3). These specific dates were chosen as they reflect a shift in mobility due to the COVID-19 pandemic in Ecuador.

With Sentinel-5P data, an additional analysis was performed in order to have a better spatial resolution and eliminate the interference of clouds or other weather conditions; the Empirical Bayesian Kriging (EBK) method was used to obtain images of 0.03 km^2 per pixel [27,29]. On the other hand, for the calculation of statistics we worked at the level of raw pixel data of O_3 and NO_2 which were considered values > 0.70 and > 0.75 respectively, which eliminates cloud-coverage distortions, errors and problematic recoveries [29, 37–39].

2.4. Data normalization

Due to the nature of the data (in situ and Sentinel 5P) it is not possible to equate their units, however, so that they can be comparable to each other, they were normalized between 0 and 1 using the formula (eq. (1)):

$$X\ norm = \frac{X - Xmin}{Xmáx - Xmin} \tag{1}$$

where Xnorm = the normalized value, X = the original value, Xmin = the minimum value of the data set, Xmax = the maximum value of the data set.

2.5. Data analysis

2.5.1. Linear Regression Model and spatio-temporal analysis

To determine the association between ground-based and satellite data, a LRM was specifically employed. These regression analyses were performed using R-4.3.0 in RStudio 2022.07.1. The LRM, widely recognized for its simplicity [40], was used to calculate the coefficients of determination (R^2) and the similarity (p-value) between the two datasets. The dependent variable in this case is the ground-based data, denoted as Y. The equation (eq. (2)) used to construct the model is described below:

$$Y = \beta + \beta_i X_i + \varepsilon \tag{2}$$

Where Y represents the dependent variable (ground-based data), β corresponds to the intercept, β_i represents the coefficient, X_i represents the independent variables (satellite data) in the equation and ε represents the error.

Moreover, ground and satellite data from 2019 to 2020 were analyzed to evaluate their temporal behavior before and during the COVID-19 pandemic. The analysis used Python 2.9.0 software in Google Collaboratory (https://colab.research.google.com/).

2.5.2. Intraclass correlation coefficient (ICC)

On the other hand, although the R^2 coefficient evaluates the degree of association between two variables, it does not examine the

Table 3
Sentinel-5P satellite data characteristics.

Satellite	Sensor	Polluant	Product	Frequency	Typical Recovery Range	Acquisition Period
Sentinel-5P	TROPOMI	NO_2	L3_NO2__	Monthly	0–0,0002	01/2019-12/2020
		O_3	L3_O3_TCL	Monthly	0–0,36	01/2019-12/2020

level of agreement and concordance between them. Additional information is required to interpret it correctly. A low correlation could lead to the conclusion that there is no association, however, this association could be firm but not of a linear nature [41]. To analyze the concordance between the data, the ICC and the Bland-Altman graphical method have been used, applied through the IBM SPSS Statistics 27 software.

The ICC evaluates the degree of agreement or consistency between means, whose variance can be attributed to variations between instruments that perform measurements on the same sample [42]. This coefficient is widely used in statistical analysis and validation of environmental studies [43–45]. The ICC of Absolute Agreement (ICCa) was used (eq. (3)), considering any difference between measurements as a mismatch, regardless of its type. Furthermore, it tells us that values greater than 0.5 are considered acceptable [46]. To calculate this coefficient, we use the following equation:

$$ICC_a = \frac{\sigma_p^2}{\sigma_p^2 + \sigma_{error}^2} \tag{3}$$

where σ_p^2 = variance, and σ_{error}^2 = variance of the experimental error. The evaluation of the consistency of the instrument measurements is reported using the scale proposed by Landis and Koch [47].

Bland and Altman propose a standard approach for assessing agreement between two measurement methods [48]. This approach, known as "Limits of Agreement," is based on determining whether points are located near the zero line, indicating a high agreement level between the methods. The analysis represents the differences between the measurements of both methods concerning their mean through a scatter plot while adhering to the pre-calculated limits [49,50]. The limits of agreement are determined using the following equations (eq. (4) and eq. (5)):

$$LL = \overline{X} - 1.96 \bullet SD \tag{4}$$

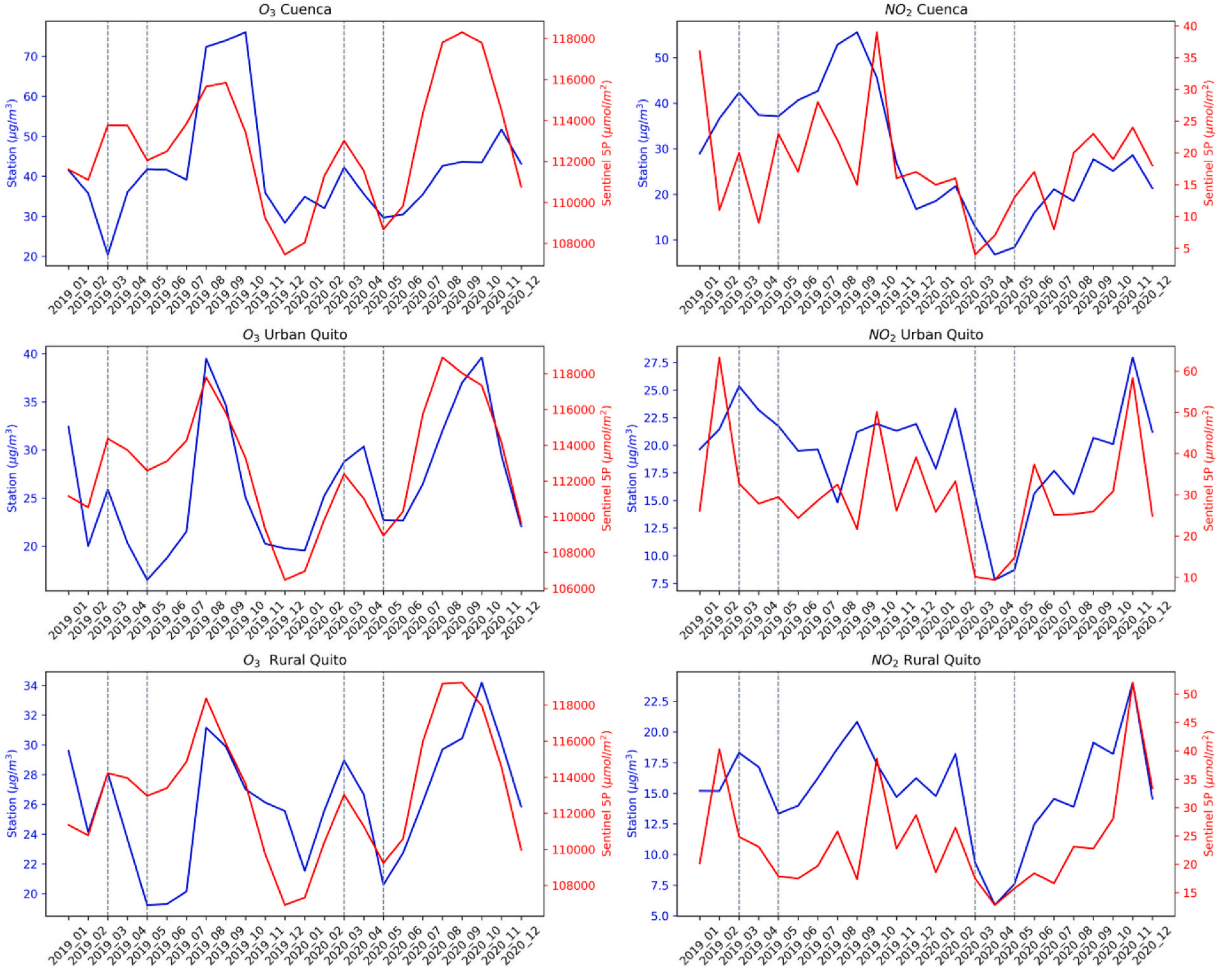

Fig. 2. Behavior of ground-based vs Sentinel-5P data for O_3 and NO_2 in the cities of Quito and Cuenca during 2019 and 2020.

$$UL = \overline{X} + 1.96 \bullet SD \quad (5)$$

Where LL = Lower limit, UL = Upper Limit; $\overline{X}$ = mean of the difference and SD = standard deviation of the difference. In the field of environmental studies, this analysis has been used to assess the agreement between satellite and ground measurements data [51] and for the validation of predictive models [52,53].

2.5.3. Bland and Altman's graphical method

The graphical method of Bland and Altman was employed to analyze the concordance of the measured data, using IBM SPSS Statistics 27 software. This method regards a zero difference between measurements as the ideal agreement. Consequently, in this context, the mean difference and its limits can also be found close to zero [54].

3. Results

3.1. Spatial-temporal and statistical analysis

In Cuenca, O_3 ground data recorded in 2020 were generally lower than those in 2019, except for the months of March, November, and December, which recorded higher values. In Quito, on the other hand, the values recorded in 2020 are higher than those of 2019 except for January and August. Sentinel-5P data show the same behavior for both cities, with higher concentrations in 2020 compared to those recorded in 2019 starting in June. Ground-based and Sentinel-5P data indicate a decrease in the concentration of this gas during the months affected by restrictions in both cities.

In 2019, elevated levels of NO_2 were recorded during March and from June to October, exceeding the limit established by the Ambient Air Quality Standard (AQS) and the WHO guidelines (40 μg m^{-3}) [36,55]. Conversely, in 2020, NO_2 concentrations were lower than those in 2019. Both data sets (Quito and Cuenca) show similar behavior during 2020, recording slight divergences from May to July; the annual average remains within the regulatory limits. In comparison, the data from 2019 show more significant differences in their behavior. Lower concentrations of gases are observed in the rural area of Quito compared to its urban area. This is especially notable for nitrogen dioxide (NO_2), where Sentinel-5P measurements show greater sensitivity (Fig. 2).

The maximum, minimum, and mean values provided by the monitoring stations and the Sentinel-5P satellite were analyzed, which are detailed in Table 4. In general, both data sets agree on the period in which the maximum and minimum values were recorded, or they are found in close time intervals.

According to the reports provided by the EMOV EP of Cuenca, it is determined that the pollutants analyzed in 2019 presented annual means lower than those established by the AQS and the values recommended by the WHO. However, there were exceptions in the case of NO_2, which exceeded the threshold value of 40 μg m^{-3} in some stations and months. In the corresponding report for 2020, all annual means were below the limits established. Similarly, the city of Quito recorded monthly NO_2 values that exceeded the regulations; however, the annual mean did not surpass the established limit.

The medians (Q2) and means of the data show small differences, attributed to the natural variability of the data, but insufficient to conclude the existence of a skewed distribution; the tails of the O_3 data present a slight platykurtic distribution, which suggests greater uniformity of the data; while for NO_2 they show a leptokurtic distribution, indicative of greater variability or the presence of unusual events in the data. For both gases the behavior differs at the Cuenca station. For the most part, the data show a positively asymmetric distribution, indicating a concentration of data towards the left side and upper extreme values scattered to the right side.

In order to visualize the variations in O_3 concentrations over time, box plots are used. For the city of Cuenca, the Sentinel-5P records an annual mean of 112519.7 μmol m^{-2} in 2019, slightly increasing to 112994.9 μmol m^{-2} in 2020 (Fig. 3b), representing a 0.42% increase in emissions. On the other hand, the station shows an annual mean of 45.25 μg m^{-3} in 2019, which decreases to 38.75 μg m^{-3} in 2020 (Fig. 3a), indicating a significant 14.4% reduction in emissions. It is worth noting that both values fall within limits established by the regulation, which is 100 μg m^{-3} [56].

When comparing the interquartile ranges (IQRs), it can be observed that the data from the stations in 2020 present a more

Table 4
Statistics of Ground-based (μg m^{-3}) and Sentinel-5P (μmol m^{-2}) data (Min: Minimum, Max: Maximum, Std: Standard Deviation).

	O_3				NO_2			
	Cuenca		Quito		Quito		Cuenca	
	Sentinel-5P	Ground-base	Sentinel-5P	Ground-base	Sentinel-5P	Ground-base	Sentinel-5P	Ground-base
Min	107458	20.45	106643.5	17.53	10.7	7.08	4,00	6.79
Q1	111015.25	35.34	110316.47	21.83	22.81	16.45	14.5	18.55
Q2	112752.5	40.34	112970.31	25.59	25.19	18.66	17	27.3
Q3	114377	43.21	114814.62	30.08	30.03	20.14	22.25	38.22
Máx	118311	76.03	119006.75	37.57	56.00	26.48	39,00	55.58
Mean	112757	41.9	112879.39	26.15	27.9	17.85	18,21	28.76
Std	3013.7	13.97	3463.77	5.60	11.05	4.2	8.27	13.44
Kurtosis	−0.53	1.84	−0.7	−0.67	1.89	1.79	1.1	−0.69
Skewness	0.15	1.43	0.1	0.53	1.25	−0.89	0.78	0.32

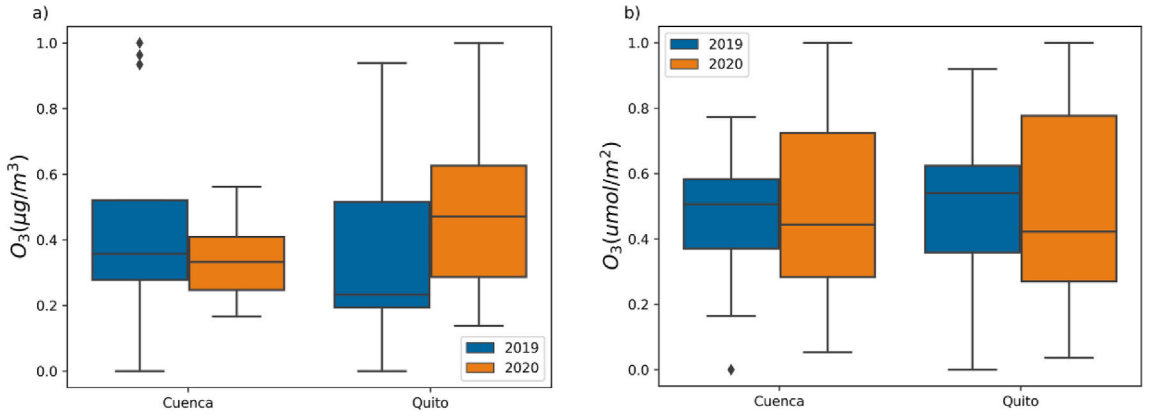

Fig. 3. Box Plots of O_3 concentrations recorded by a) Ground-based and b) Sentinel-5P stations during the years 2019 and 2020. The box represents the interquartile range (IQR), which spans from the first quartile (Q1) to the third quartile (Q3) and contains the middle 50% of the data. The horizontal line inside the box indicates the median of the data set. The whiskers of the box extend to the most extreme values within a range calculated based on IQR; points that fall outside these limits are considered outliers.

concentrated distribution and are in a lower range due to the decrease in concentration. Outlier data were recorded in 2019, while in 2020, no extreme values were observed, not even within the quartiles. This is evident from the closeness of the whiskers to the box. As for the Sentinel-5P data, the distribution in 2020 is much broader, indicating extreme values, but all are within the expected range, thus ruling out outliers and corroborating the generated increase.

In 2019, Sentinel-5P recorded a mean of 112815.8 μmol m^{-2} in Quito, slightly increasing to 112943 μmol m^{-2} in 2020 (Fig. 3b). This increase represents a 0.11% rise in concentrations. The measurement station recorded an annual mean of 27.46 μg m^{-3} in 2020, higher than the average of 24.84 μg m^{-3} recorded in 2019 (Fig. 3a), implying a 10.5% increase in emissions of this pollutant. During 2020, Sentinel-5P recorded values with a wider dispersion, indicated by a more extensive interquartile range compared to the 2019 data. However, overall, the medians of the data were lower in 2020, except for the ground-based data in Quito. The box plots highlight the increase in O_3 concentrations for 2019 and 2020. However, neither of the two years presents any outliers, meaning all values fall within the expected limits.

In the city of Cuenca, Sentinel-5P recorded a mean NO_2 concentration of 21.08 μmol m^{-2} in 2019, which decreased to 15.33 μmol m^{-2} in 2020 (Fig. 4b), reflecting a decrease rate of 27.3%. Meanwhile, the monitoring station reported an annual mean of 38.63 μg m^{-3} in 2019 and 18.89 μg m^{-3} in 2020 (Fig. 4a), evidencing a reduction of 51% in NO_2 emissions. In comparison, the IQRs of Sentinel-5P are only slightly wider than those recorded by the station. In 2019, both data sets exhibited extreme values and outliers distribution. However, examining the location of the central values in both cases confirms the decrease in concentrations in the year 2020 (Fig. 4).

In Quito, Sentinel-5P recorded an annual mean of 30.2 μmol m^{-2} for NO_2 in 2019, which decreased to 25.64 μmol m^{-2} in 2020 (Fig. 4b), translating into a decrease rate in emissions of 15.1%. On the other hand, the monitoring station recorded an annual mean of 19.28 μg m^{-3} in 2019, decreasing to 16.43 μg m^{-3} in 2020 (Fig. 4a), indicating a reduction rate of 14.7%. For Quito, the satellite data registers outliers during both years. However, the IQR shows a highly constrained data distribution, and the recorded decreases are

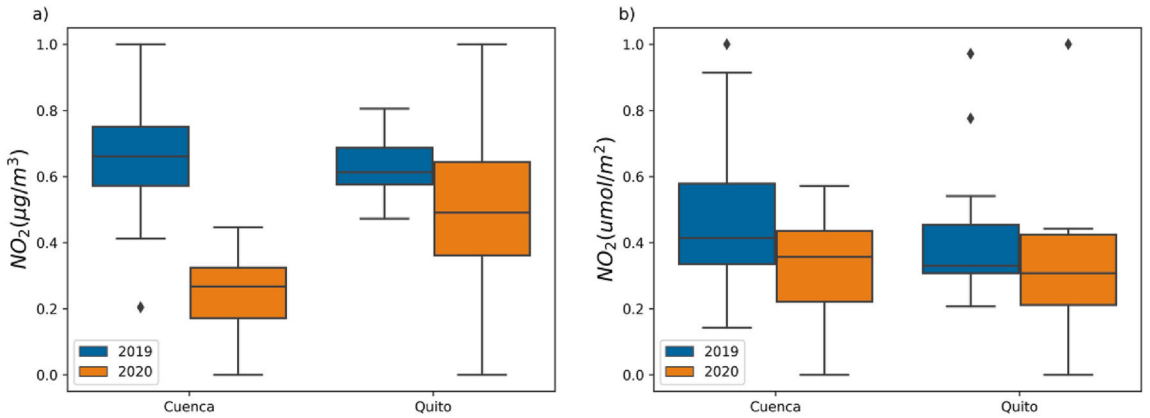

Fig. 4. Box plots of NO_2 concentrations recorded by a) Ground-based stations and b) Sentinel-5P during the years 2019 and 2020. The box represents the interquartile range (IQR), which spans from the first quartile (Q1) to the third quartile (Q3) and contains the middle 50% of the data. The horizontal line inside the box represents the median of the data set. The whiskers on the box extend to the most extreme values within a range calculated based on IQR; points outside these limits are considered outliers.

evident in both cases.

Fig. 5 displays the spatial distribution of NO_2 in the city of Quito. The concentrations of this pollutant change during the restriction periods, showing a decrease compared to the year 2019. On the other hand, in the city of Cuenca (Fig. 5), despite the mean concentrations of this gas being similar in both years, a significant decrease in its presence in the troposphere is observed during the restriction period.

In relation to the O_3 concentrations during mobility restrictions, a significant decrease of this pollutant can be noted in the cities of Quito and Cuenca (Fig. 6). This observation aligns with Fig. 2, both in the data gathered from ground-based stations and those obtained via satellite.

3.2. Relationship of Sentinel-5P data to ground-based data

As depicted in Fig. 2, both datasets exhibit similar patterns and trends. The disparities observed between the Ground-based and Sentinel-5P data can be attributed to the variance in the detection heights of the gases. While the stations record data at the surface concentrations, Sentinel-5P provides the mean value across the entire vertical column. Additionally, the datasets showcase maximum and minimum concentrations during the same or adjacent months, with the Quito data displaying the highest similarity. In order to establish a correlation between the Sentinel-5P data and those provided by EMOV in Cuenca and REMMAQ in Quito (n = 216), normalized data is utilized. Linear regressions are conducted to determine the adjusted R^2 value and Pearson's Correlation Coefficient

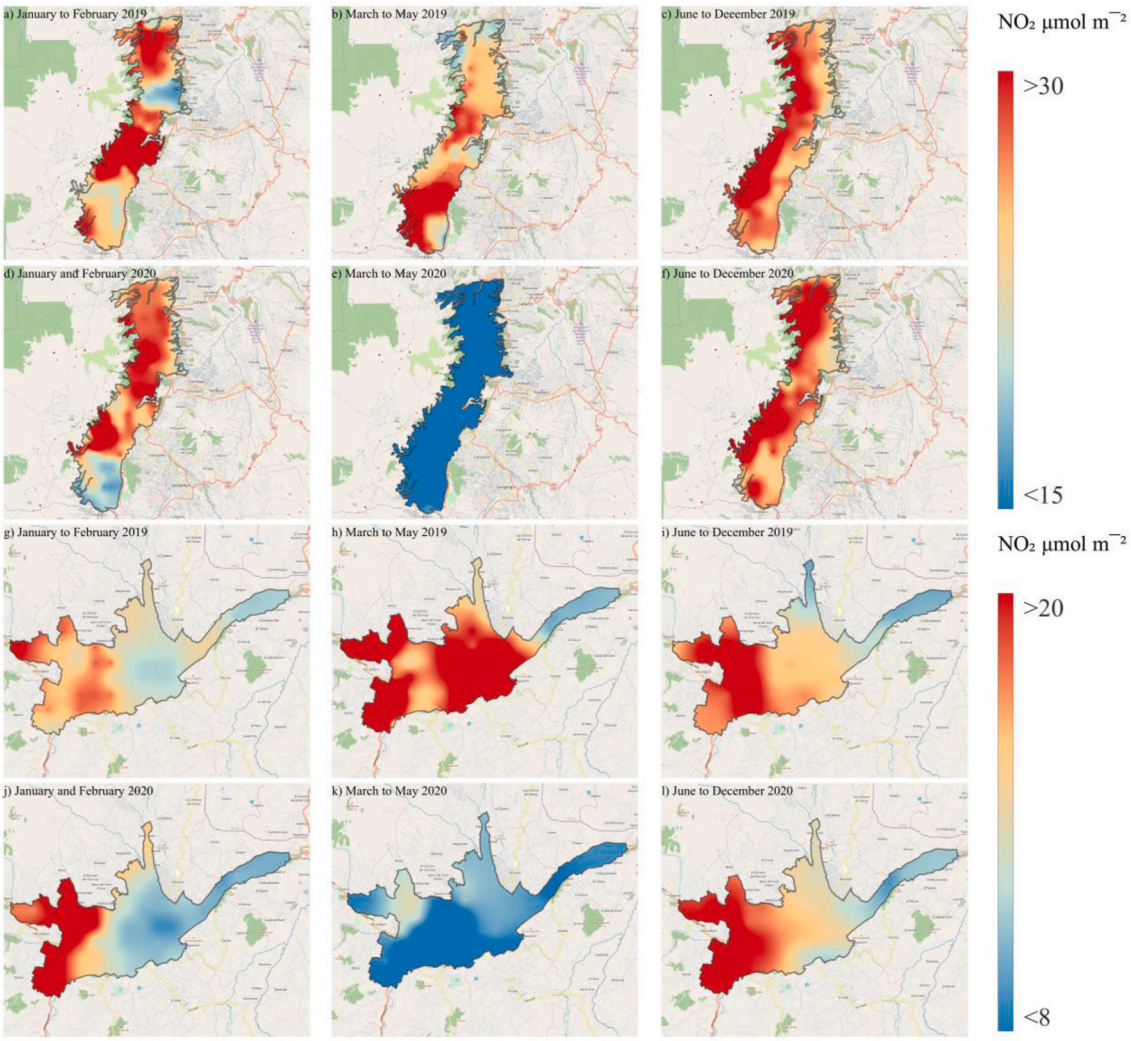

Fig. 5. Spatial distribution of NO_2 in the cities of Quito and Cuenca during various periods: a) Quito (January–February 2019), b) Quito (March–May 2019), c) Quito (June–December 2019), d) Quito (January–February 2020), e) Quito (March–May 2020), f) Quito (June–December 2020), g) Cuenca (January–February 2019), h) Cuenca (March–May 2019), i) Cuenca (June–December 2019), j) Cuenca (January–February 2020), k) Cuenca (March–May 2020), i) Cuenca (June–December 2020).

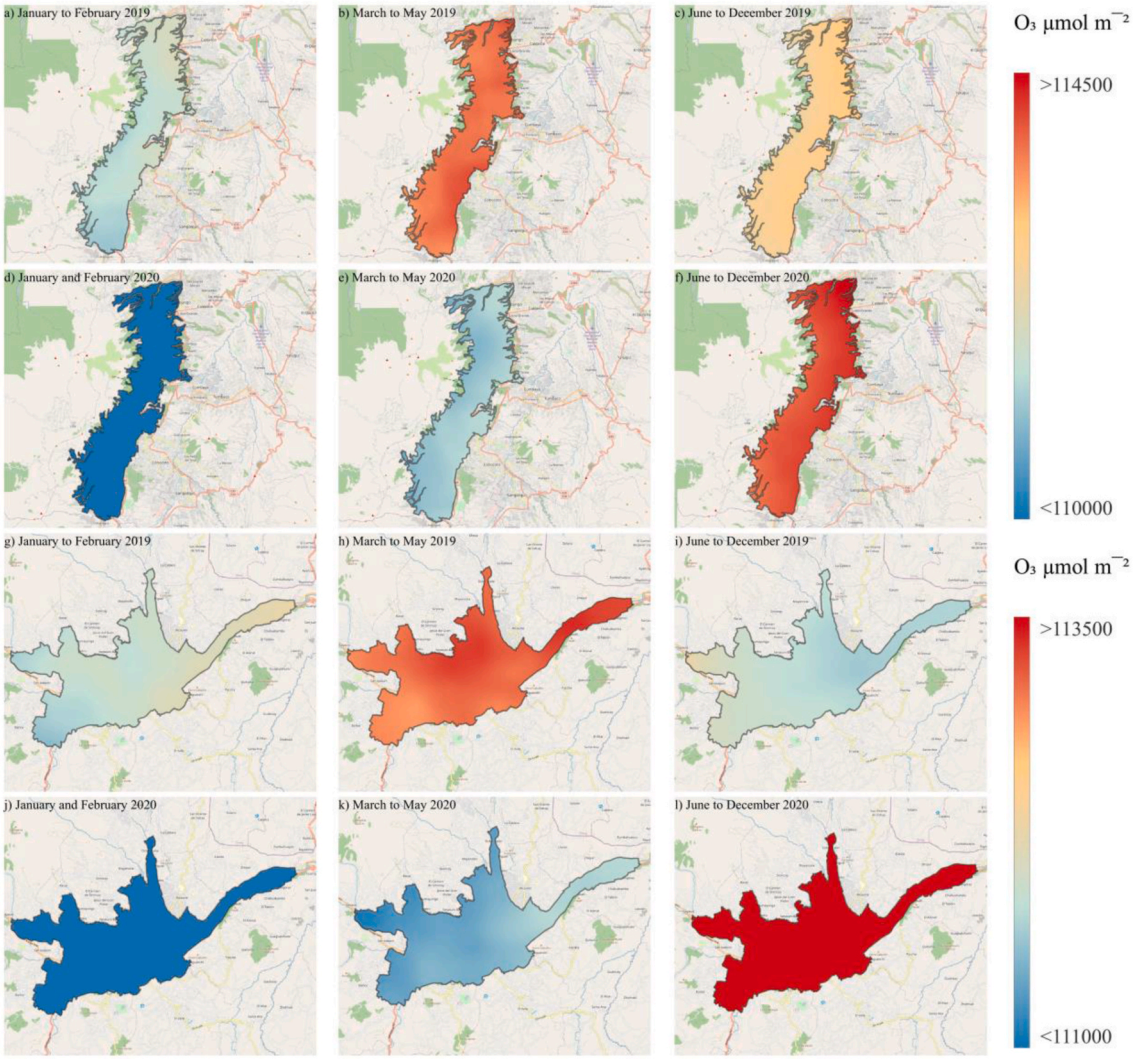

Fig. 6. Spatial distribution of O_3 in the cities of Quito and Cuenca during various periods: a) Quito (January–February 2019), b) Quito (March–May 2019), c) Quito (June–December 2019), d) Quito (January–February 2020), e) Quito (March–May 2020), f) Quito (June–December 2020), g) Cuenca (January–February 2019), h) Cuenca (March–May 2019), i) Cuenca (June–December 2019), j) Cuenca (January–February 2020), k) Cuenca (March–May 2020), i) Cuenca (June–December 2020).

(r) using RStudio (Fig. 7).

Firstly, the complete dataset was examined, and subsequently analyzed separately, using the city as the differentiation criterion. For Cuenca, the relationships were found to be low, which could be attributed to the small sample size, as outlier values could cause significant variations in the determined coefficients.

For the total dataset, lower relationships were observed than in the differentiated data (Table 5). Regarding the data for Cuenca, R^2 value of 0.73 was obtained for both gases, indicating a high association between the variables. As for the mean data of the city of Quito, R^2 value of 0.83 was recorded, which points to an almost perfect degree of association between the measurements. According to the RMSE values, a reasonable accuracy can be attributed to the models in terms of fit to the data, while the recorded MBE values suggest that the models do not have pronounced biases and tend to make fairly accurate predictions on average.

According to Levene's statistics based on the mean, the significance value ($p \geq 0.05$) indicates that the variances of the station data with those collected by Sentinel-5P are equal, both groups are homogeneous (Table 6). The results of the ANOVA between one-factor groups accept the null hypothesis and indicate equality of the group means.

Table 7 shows the coefficients obtained for each of the stations in the city of Quito, all stations show similar correlations for the gases analyzed. The Belisario station shows the best correlations between the data for both O_3 and NO_2, the Guamaní station showed a good correlation for O_3 and Carapungo for NO_2.

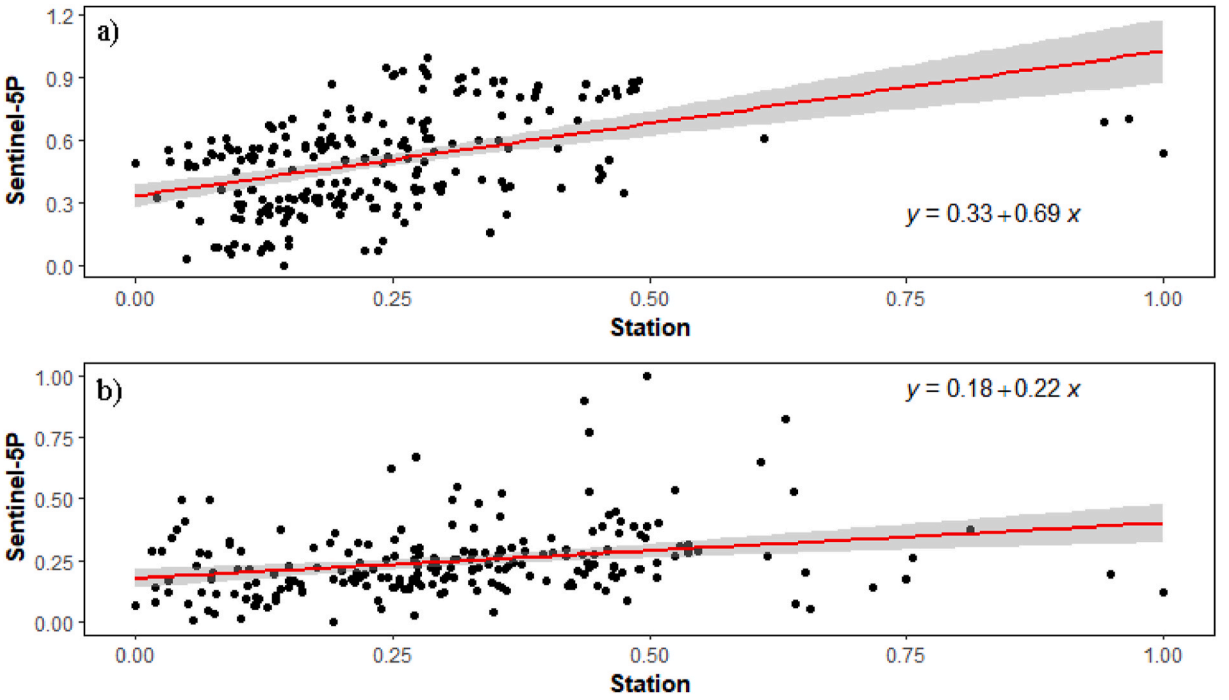

Fig. 7. Linear regression for Sentinel-5P vs ground-based data: a) O_3 data, b) NO_2 data.

Table 5
Values of Coefficient of Determination (R^2), Root Mean Square Error (RMSE), Mean Biased Error(MBE), and P-Value for Sentinel-5P data vs. Ground-based data.

	Total Data				Cuenca				Quito			
	R^2	**RMSE**	**MBE**	**p-value**	**R^2**	**RMSE**	**MBE**	**p-value**	**R^2**	**RMSE**	**MBE**	**p-value**
O_3	0.74	0.13	0.01	2e-16***	0.72	0.23	0.04	4.2e-8***	0.83	0.18	0.03	2e-16***
NO_2	0.66	0.20	0.04	2e-16***	0.72	0.26	0.05	4.6e-8 ***	0.74	0.25	0.07	2e-16***

Signif. codes: 0 '***' 0.001 '**' 0.01 '*' 0.05 '.' 0.1 ' ' 1.

Tabla 6
Levene statistics based on mean and sample values One-way between-group ANOVA.

		Levene	p-value	F	p-value
Cuenca	O_3	1.25	0.269	1.73	0.195
	NO_2	1.49	0.23	0.358	0.553
Quito	O_3	0.005	0.946	0.842	0.364
	NO_2	0.078	0.781	6.842	0.012

Table 7
Values of R^2, RMSE and r for Senrinel-5P data for the Quito stations.

	R^2		RMSE		**MBE**	
	O_3	**NO_2**	**O_3**	**NO_2**	**O_3**	**NO_2**
BEL	0.81	0.82	0.25	0.24	0.015	0.08
CAM	0.77	0.69	0.29	0.43	−0.005	0.18
CAR	0.77	0.77	0.24	0.28	0.04	0.11
CEN	0.76	0.76	0.28	0.30	0.01	0.12
CHI	0.75	0.72	0.30	0.31	0.05	0.14
COT	0.77	0.41	0.25	0.41	0.01	0.06
GUA	0.85	0.75	0.20	0.25	0.01	0.05
TUM	0.77	0.72	0.28	0.29	0.05	0.12

3.3. Intraclass correlation coefficient (ICC)

The ICC of absolute agreement was calculated, which considers any discrepancy between measurements, whether of constant, proportional, or other types, as a lack of concordance. The ICC was applied to the normalized data from the cities of Cuenca and Quito, obtaining the following results (Table 8).

3.4. Bland and Altman's graphical method

For the dataset corresponding to the city of Cuenca (Table 9), the Bland and Altman method revealed a mean bias ± SD between the measurements of Sentinel-5P and the city's automatic monitoring station for O_3 of -0.100 ± 0.276, with concordance limits of -0.629 and 0.429 (Fig. 8a). The concordance limits established for NO_2 were -0.490 and 0.580, with a mean bias ± SD between the measurements of Sentinel-5P and the monitoring station of the City of Cuenca of 0.044 ± 0.273 (Fig. 8b). The evaluation determines that, with 95% of the points close to the line representing the mean bias and within the agreement limits, the reliability of Sentinel-5P data is guaranteed.

The Bland and Altman graphical method was applied for the data recorded in Quito (Table 8). For O_3, the plot showed the mean ± SD bias between Sentinel-5P measurements and in situ data as -0.079 ± 0.210, and the limits of agreement were -0.490 and 0.330 (Fig. 9a). For NO_2, the mean ± SD bias between Sentinel-5P measurements and in situ, data was 0.19 ± 0.21, and the limits of agreement were set at -0.230 and 0.620 (Fig. 9b).

The evaluation of these results suggests that the differences are close to the line representing the mean bias. Within the agreement limits, the reliability of the data provided by Sentinel-5P is ensured. Moreover, it can be determined that the differences obtained between the data do not show any trend, ruling out the presence of systematic errors or interferences of any other kind in the measurement of values..

4. Discussion

The results obtained support the efficiency and relevance of Sentinel-5P in the continuous monitoring of air quality in cities in Ecuador, using the collateral effect of COVID-19 on air quality during 2020. NO_2 concentrations are directly linked to linear sources, for which the decrease in vehicle traffic had a notable influence. The comparative analysis between a conventional year and another marked by pandemic restrictions, with emphasis on the critical months of confinement, showed a spatio-temporal evolution of air pollution influenced by the restriction measures implemented.

The regression model applied satisfactorily corrected the spatial deficiencies of the monitoring network, validated by calculating the CCI and graphical representation of Bland and Altman. This highlights the sensitivity of Sentinel-5P regarding detection and modelling of changes in the concentration of air pollutants in the vicinity of the surface [58,59] and as noted by Jeong and Hong [60], in identifying contamination hotspots, a crucial aspect to strengthen the monitoring air pollutants in cities that lack monitoring networks or have incomplete networks.

Historical data collected by EMOV EP indicates an increasing trend in NO_2 concentration since 2012. However, restrictive measures managed to mitigate this trend with significant decreases in average annual concentrations. In Quito, a decrease of 15.1% by Sentinel-5P and 14.7% by the stations is observed, corroborating what has been documented by Mejia et al. [27], Zalakeviciute et al. [15,29], and Zambrano & Ruano [61]. Similarly, significant increases (0.11% for Sentinel 5P and 10.5% for the stations) of O_3 are recorded, which support what was reported by Carzola et al. [62], and Pacheco et al., [63]. In Cuenca, an increase of 0.42% in the concentration of O_3 was observed by Sentinel-5P, while the stations indicated reductions of 14.4% for this gas and 27.3% and 51% of NO_2 by Sentinel-5P and the stations respectively.

These findings align with those of Sicard et al. [64], who documented decreases of 53% in NO_2 concentrations in Nice, Rome, Valencia and Wuhan, and 30% in Turin. These cities also experienced an increase in O_3 levels. Anbari et al. [65] reported a 12.2% increase in annual O_3 concentrations in the city of Khorramabad (Iran), attributed to the decrease in NO_2 due to lockdown measures. Tudor [66] also revealed that O_3 levels increased during the first COVID-19 lockdown in the United Kingdom, leading to more severe pollution from March to June 2020. Similar findings have been reported in Spain [67,68]; Previously other authors had already documented this effect [69,70].

Although currently the annual pollution regulations have not been exceeded, daily records have already exceeded these thresholds; In addition to highlighting the importance of satellite data, this study supports previous analyzes that have established relationships between the decrease in pollution and the reduction in mobility, establishing an informative precedent that can be used as a basis for the implementation of future measures aimed at controlling pollution levels and that, in accordance with Art. 14 of the Constitution of Ecuador, guarantee all citizens the right to live in a healthy and ecologically balanced environment. Future studies are encouraged to use these data in statistical techniques such as geographical weighted regression (GRW) that include spatial variability or regression algorithms that make predictions with a broader set of variables such as Random Forest.

5. Conclusions

This study analyzed Sentinel-5P satellite data sets from 2019 to 2020. To validate the derived data on O_3 and NO_2, information from automatic stations monitoring surface concentrations and urban air quality was utilized. The results exhibited a significant correlation (O_3, $R^2 = 0.72$ for Cuenca and 0.83 for Quito; NO_2, $R^2 = 0.72$ for Cuenca and 0.74 for Quito).

Table 8
Intraclass Correlation Coefficient (ICC) for Sentinel-5P vs. Ground-based data.

	Cuenca			Quito		
	ICC value	**ICC Mean**	**Significance**	**ICC value**	**ICC Mean**	**Significance**
O_3	0.43	0.60	0.011	0.415	0.586	0.001
NO_2	0.43	0.60	0.015	0.404	0.576	0.001

The ICC for O_3 and NO_2 recorded values of approximately 0.6 in the mean measurements and with a statistical significance of $p < 0.05$, from which it was determined, as proposed by Ref. [57], that by having an ICC between 0.41 and 0.75 the agreement between the Ground-Based data and the Sentinel-5P data for O_3 and NO_2 is good.

Table 9
Statistics for differences between data for the city of Cuenca.

	Median	Standard deviation	Mean standard error	Upper Limit	Lower Limit
O_3	−0.10	0.276	0.056	0.43	−0.63
NO_2	0.04	0.273	0.056	0.58	−0.49

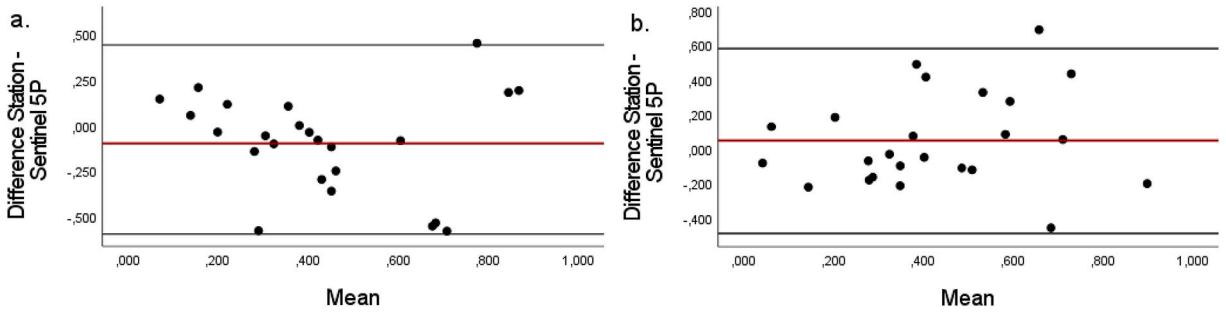

Fig. 8. Bland and Altman graphical method for Ground-based vs Sentinel-5P measurements in the city of Cuenca. a) O_3, b) NO_2. The black lines correspond to the upper and lower limits, while the red line corresponds to the median their values are detailed in Table 9. (For interpretation of the references to colour in this figure legend, the reader is referred to the Web version of this article.)

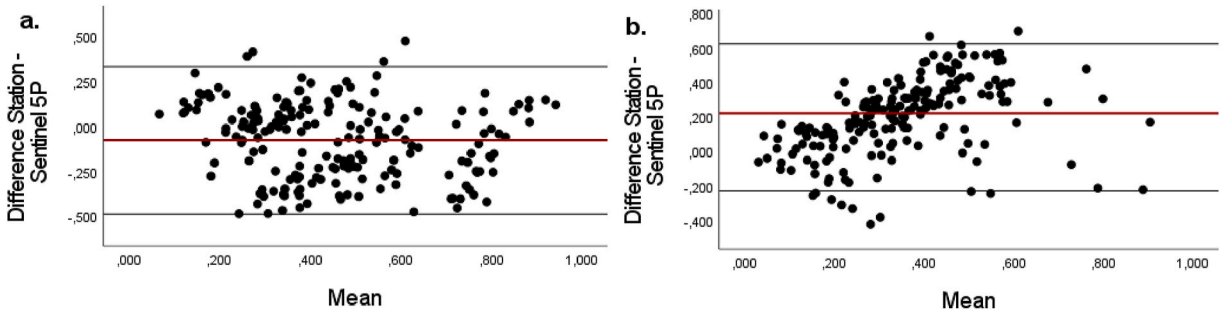

Fig. 9. Bland and Altman's graphical method for Ground-based vs Sentinel-5P measurements in Quito. a) O_3, b) NO_2. The black lines correspond to the upper and lower limits, while the red line corresponds to the median their values are detailed in Table 10. (For interpretation of the references to colour in this figure legend, the reader is referred to the Web version of this article.)

Table 10
Statistics for data differences for Quito.

Differences	Mean	Standard deviation	Mean standard error	Upper Limit	Lower Limit
O_3	−0.079	0.210	0.015	0.33	−0.49
NO_2	0.194	0.219	0.016	0.62	−0.23

Additionally, the impact of COVID-19 mobility restrictions on gas concentrations was examined. The months of interest were March, April, and May when mobility was heavily restricted nationwide. Both data sets indicated a decrease in NO_2 concentrations and an increase in O_3 concentrations, particularly during these months, in both cities.

This study highlights the usefulness of Sentinel-5P data for air quality studies and assesses the impact of mobility restrictions on air pollution in Quito and Cuenca. Future research can consider additional factors, such as meteorological parameters, to further investigate the convergence of pollutants in specific areas of the cities. The findings provide valuable information for authorities, health agencies, and academics interested in improving urban development to prioritize health and quality of life.

Finally, it has been determined that the Sentinel-5P satellite can effectively detect anomalies in NO_2 and O_3 concentrations. It is essential to acknowledge that previous studies have access to more extensive monitoring networks than those available in Ecuador. Thus, the significance of our research lies in its applicability to developing countries that may have limited monitoring infrastructure for urban planning purposes.

Author contributions

Rasa Zalakeviciute: Writing – review & editing. Gina Faican: Writing – original draft, Investigation. Danilo Mejía C: Writing – review & editing, Writing – original draft, Visualization, Project administration, Investigation, Conceptualization. Carlos Matovelle: Writing – review & editing, Funding acquisition. Santiago Bonilla: Writing – review & editing. Jose Sobrino: Writing – review & editing, Project administration

Data availability statement

The data associated with this research have not been deposited in the public repository. The data will be available upon request to the authors.

Declaration of competing interest

The authors declare that they have no known competing financial interests or personal relationships that could have appeared to influence the work reported in this paper.

References

[1] Y. Guan, et al., Summer O3 pollution cycle characteristics and VOCs sources in a central city of Beijing-Tianjin-Hebei area, China, Environ. Pollut. 323 (Apr. 2023) 121293, https://doi.org/10.1016/j.envpol.2023.121293.
[2] G. Huang, Y. Jiang, W. Zhou, S.T.A. Pickett, B. Fisher, The impact of air pollution on behavior changes and outdoor recreation in Chinese cities, Landsc. Urban Plann. 234 (Jun) (2023), https://doi.org/10.1016/J.LANDURBPLAN.2023.104727.
[3] M.M.M.F. Jion, et al., A critical review and prospect of NO2 and SO2 pollution over Asia: hotspots, trends, and sources, Sci. Total Environ. 876 (Jun. 2023) 162851, https://doi.org/10.1016/J.SCITOTENV.2023.162851.
[4] W. Ni, X. Hu, Y. Ju, Q. Wang, Air pollution and indoor work efficiency: evidence from professional basketball players in China, J. Clean. Prod. 399 (May 2023) 136644, https://doi.org/10.1016/J.JCLEPRO.2023.136644.
[5] T. Feng, et al., Air pollution control or economic development? Empirical evidence from enterprises with production restrictions, J. Environ. Manag. 336 (Jun) (2023), https://doi.org/10.1016/J.JENVMAN.2023.117611.
[6] Y. Wang, et al., Greenness modifies the association between ambient air pollution and cognitive function in Australian adolescents, but not in mid-life adults, Environ. Pollut. 324 (May 2023), https://doi.org/10.1016/J.ENVPOL.2023.121329.
[7] P. Sokharavuth, et al., Air pollution mitigation assessment to inform Cambodia's first clean air plan, Environ. Res. 220 (Mar) (2023), https://doi.org/10.1016/J.ENVRES.2023.115230.
[8] H. Wang, R. Tang, Y. Liu, Potential health benefit of NO2 abatement in China's urban areas: inspirations for source-specific pollution control strategy, Lancet Reg Health West Pac 24 (Jul. 2022) 100482, https://doi.org/10.1016/J.LANWPC.2022.100482.
[9] L. Wang, T. Shi, H. Chen, Air pollution and infant mortality: evidence from China, Econ. Hum. Biol. 49 (Apr. 2023) 101229, https://doi.org/10.1016/J.EHB.2023.101229.
[10] P. Prunet, O. Lezeaux, C. Camy-Peyret, H. Thevenon, Analysis of the NO2 tropospheric product from S5P TROPOMI for monitoring pollution at city scale, City and Environment Interactions 8 (Nov. 2020) 100051, https://doi.org/10.1016/J.CACINT.2020.100051.
[11] R. Wang, et al., New insight into formation mechanism, source and control strategy of severe O3 pollution: the case from photochemical simulation in the Wuhan Metropolitan Area, Central China, Atmos. Res. 284 (Mar. 2023) 106605, https://doi.org/10.1016/J.ATMOSRES.2023.106605.
[12] Q. Qi, S. Wang, H. Zhao, S.H. Kota, H. Zhang, Rice yield losses due to O3 pollution in China from 2013 to 2020 based on the WRF-CMAQ model, J. Clean. Prod. 401 (May 2023) 136801, https://doi.org/10.1016/j.jclepro.2023.136801.
[13] M. in 't Veld, et al., Understanding the local and remote source contributions to ambient O3 during a pollution episode using a combination of experimental approaches in the Guadalquivir valley, southern Spain, Sci. Total Environ. 777 (Jul. 2021) 144579, https://doi.org/10.1016/j.scitotenv.2020.144579.
[14] J. Cevallos, Estimación del consumo de combustibles en el transporte terrestre en Ecuador, Documentos de Trabajo CEPROEC, 2015 [Online]. Available: https://ideas.repec.org/p/cpe/cpewps/2015_05.html. (Accessed 21 March 2023).
[15] R. Zalakeviciute, et al., Drastic improvements in air quality in Ecuador during the COVID-19 outbreak, Aerosol Air Qual. Res. 20 (8) (2020) 1783–1792, https://doi.org/10.4209/aaqr.2020.05.0254.
[16] F. Granella, L. Aleluia Reis, V. Bosetti, M. Tavoni, COVID-19 lockdown only partially alleviates health impacts of air pollution in Northern Italy, Environ. Res. Lett. 16 (3) (Mar. 2021) 035012, https://doi.org/10.1088/1748-9326/abd3d2.
[17] C. Jephcote, A.L. Hansell, K. Adams, J. Gulliver, Changes in air quality during COVID-19 'lockdown' in the United Kingdom, Environ. Pollut. 272 (Mar. 2021) 116011, https://doi.org/10.1016/j.envpol.2020.116011.
[18] H. Pacheco, S. Díaz-López, E. Jarre, H. Pacheco, W. Méndez, E. Zamora-Ledezma, NO2 levels after the COVID-19 lockdown in Ecuador: a trade-off between environment and human health, Urban Clim. 34 (Dec. 2020) 100674, https://doi.org/10.1016/J.UCLIM.2020.100674.
[19] Y.J. Wong, et al., Quantification of COVID-19 impacts on NO2 and O3: systematic model selection and hyperparameter optimization on AI-based meteorological-normalization methods, Atmos. Environ. 301 (May 2023) 119677, https://doi.org/10.1016/j.atmosenv.2023.119677.

[20] A. Richter, J.P. Burrows, H. Nüß, C. Granier, U. Niemeier, Increase in tropospheric nitrogen dioxide over China observed from space, Nature 2005 437:7055 437 (7055) (Sep. 2005) 129–132, https://doi.org/10.1038/nature04092.

[21] A.P. Rudke, et al., Evaluating TROPOMI and MODIS performance to capture the dynamic of air pollution in São Paulo state: a case study during the COVID-19 outbreak, Remote Sens. Environ. 289 (May 2023) 113514, https://doi.org/10.1016/j.rse.2023.113514.

[22] Y. Shen, et al., Increased diurnal difference of NO2 concentrations and its impact on recent ozone pollution in eastern China in summer, Sci. Total Environ. 858 (Feb. 2023) 159767, https://doi.org/10.1016/j.scitotenv.2022.159767.

[23] Z. Shi, et al., Abrupt but smaller than expected changes in surface air quality attributable to COVID-19 lockdowns, Sci. Adv. 7 (3) (Jan. 2021), https://doi.org/10.1126/sciadv.abd6696.

[24] G.J.M. Velders, et al., Improvements in air quality in The Netherlands during the corona lockdown based on observations and model simulations, Atmos. Environ. 247 (Feb. 2021) 118158, https://doi.org/10.1016/j.atmosenv.2020.118158.

[25] M.I. Volke, R. Abarca-del-Rio, C. Ulloa-Tesser, Impact of mobility restrictions on NO2 concentrations in key Latin American cities during the first wave of the COVID-19 pandemic, Urban Clim. 48 (Mar. 2023) 101412, https://doi.org/10.1016/J.UCLIM.2023.101412.

[26] Y. Wang, et al., Four-Month changes in air quality during and after the COVID-19 lockdown in six megacities in China, Environ. Sci. Technol. Lett. 7 (11) (Nov. 2020) 802–808, https://doi.org/10.1021/acs.estlett.0c00605 [H. Wang.

[27] D. Mejía C, H. Alvarez, R. Zalakeviciute, D. Macancela, C. Sanchez, S. Bonilla, Sentinel satellite data monitoring of air pollutants with interpolation methods in Guayaquil, Ecuador, Remote Sens. Appl. 31 (Aug. 2023) 100990, https://doi.org/10.1016/j.rsase.2023.100990.

[28] D. Arikan, F. Yildiz, Investigation of Antalya forest fire's impact on air quality by satellite images using Google earth engine, Remote Sens. Appl. 29 (Jan. 2023) 100922, https://doi.org/10.1016/j.rsase.2023.100922.

[29] R. Zalakeviciute, et al., War impact on air quality in Ukraine, Sustainability 14 (21) (Oct. 2022) 13832, https://doi.org/10.3390/su142113832.

[30] A. Barrera, P. Cabrera-Barona, P. Velasco-Oña, A. Barrera, P. Cabrera-Barona, P. Velasco-Oña, Derechos, calidad de vida y división social del espacio en el Distrito Metropolitano de Quito, Eure 48 (144) (2022) 1–23, https://doi.org/10.7764/EURE.48.144.05.

[31] A.S. Bustamante Campoverde, Análisis de la isla de calor urbana en el entorno andino de Cuenca-Ecuador, Invest. Geográficas (70) (Dec. 2018) 167, https://doi.org/10.14198/INGEO2018.70.08.

[32] J.P.L. Nasa, NASADEM Merged DEM Global 1 arc second V001, NASA EOSDIS Land Processes DAAC 13 (2020). Feb.

[33] SENPLADES, Proyecciones Y Estudios Demográficos 2018, 2018. Ecuador.

[34] M. Kottek, J. Grieser, C. Beck, B. Rudolf, F. Rubel, World Map of the Köppen-Geiger climate classification updated, Meteorol. Z. 15 (3) (Jul. 2006) 259–263, https://doi.org/10.1127/0941-2948/2006/0130.

[35] Secretaría de Ambiente, Ubicación de estaciones, DMQ - CORPAIRE MONITOREO ATMOSFERICO REDES MANUALES Y PASIVAS, 2022. https://sites.google.com/site/redesmanualesypasivas/Home/ubicacion-de-estaciones. (Accessed 3 February 2023).

[36] E.P. Emov, "Informe de Calidad del Aire de Cuenca 2019," Cuenca, 2020 [Online]. Available: https://www.emov.gob.ec/sites/default/files/CALIDAD_DEL_AIRE_2019.pdf. (Accessed 23 April 2023).

[37] ESA, Sentinel-5 Precursor Level 2 Tropospheric Ozone - Sentinel Online, 2020. https://sentinels.copernicus.eu/web/sentinel/data-products/-/asset_publisher/fp37fc19FN8F/content/tropomi-level-2-tropospheric-ozone. (Accessed 12 February 2023).

[38] ESA, Productos de datos - misión Sentinel-5P - Sentinel Online. https://sentinels.copernicus.eu/web/sentinel/missions/sentinel-5p/data-products, 2020. (Accessed 3 August 2022).

[39] H.J. Eskes, et al., "S5P Mission Performance Centre Nitrogen Dioxide [L2_NO2__]," 02.05.00 (Mar. 2023), https://doi.org/10.5270/S5P-9bnp8q8.

[40] Y. Xu, et al., Evaluation of machine learning techniques with multiple remote sensing datasets in estimating monthly concentrations of ground-level PM2.5, Environ. Pollut. 242 (Nov. 2018) 1417–1426, https://doi.org/10.1016/j.envpol.2018.08.029.

[41] R.M. Martínez Ortega, L.C. Tuya Pendás, M. Martínez Ortega, A. Pérez Abreu, A.M. Cánovas, EL COEFICIENTE de CORRELACION de los rangos de spearman CARACTERIZACION, Rev. Habanera Ciencias Méd. 8 (2) (2009) [Online]. Available: http://scielo.sld.cu/scielo.php?script=sci_arttext&pid=S1729-519X2009000200017&lng=es&nrm=iso&tlng=es. (Accessed 2 February 2023).

[42] J. Correa-Rojas, Coeficiente de Correlación Intraclase: aplicaciones para estimar la estabilidad temporal de un instrumento de medida, Ciencias Psicológicas 15 (2) (Nov. 2021) 2318, https://doi.org/10.22235/CP.V15I2.2318.

[43] S. Buteau, et al., Comparison of spatiotemporal prediction models of daily exposure of individuals to ambient nitrogen dioxide and ozone in Montreal, Canada, Environ. Res. 156 (Jul. 2017) 201–230, https://doi.org/10.1016/J.ENVRES.2017.03.017.

[44] K. Lee, Y. Yanagisawa, J.D. Spengler, R. Davis, Assessment of precision of a passive sampler by duplicate measurements, Environ. Int. 21 (4) (Jan. 1995) 407–412, https://doi.org/10.1016/0160-4120(95)00034-I.

[45] A. Li, et al., Associations between air pollutant exposure and renal function: a prospective study of older adults without chronic kidney disease, Environ. Pollut. 277 (May 2021) 116750, https://doi.org/10.1016/J.ENVPOL.2021.116750.

[46] D. Liljequist, B. Elfving, K. Skavberg Roaldsen, Intraclass correlation – a discussion and demonstration of basic features, PLoS One 14 (7) (Jul. 2019) e0219854, https://doi.org/10.1371/journal.pone.0219854.

[47] J.R. Landis, G.G. Koch, The measurement of observer agreement for categorical data, Biometrics 33 (1) (Mar. 1977) 159, https://doi.org/10.2307/2529310.

[48] M.A. Mansournia, R. Waters, M. Nazemipour, M. Bland, D.G. Altman, Bland-Altman methods for comparing methods of measurement and response to criticisms, Glob Epidemiol 3 (Nov. 2021) 100045, https://doi.org/10.1016/J.GLOEPI.2020.100045.

[49] F. Cardemil, Comparison analysis and applications of the Bland-Altman method: correlation or agreement? Medwave 17 (1) (Jan. 2017) https://doi.org/10.5867/MEDWAVE.2016.01.6852.

[50] D. Giavarina, Understanding Bland altman analysis, Biochem. Med. 25 (2) (2015) 141, https://doi.org/10.11613/BM.2015.015.

[51] H. Wang, F.-Y. Gong, S. Newman, Z.-C. Zeng, Consistent weekly cycles of atmospheric NO2, CO, and CO2 in a North American megacity from ground-based, mountaintop, and satellite measurements, Atmos. Environ. 268 (Jan. 2022) 118809, https://doi.org/10.1016/j.atmosenv.2021.118809.

[52] A. de Nazelle, et al., Comparison of performance of land use regression models derived for Catalunya, Spain, Atmos. Environ. 77 (Oct. 2013) 598–606, https://doi.org/10.1016/j.atmosenv.2013.05.054.

[53] B. Yeganeh, M.G. Hewson, S. Clifford, A. Tavassoli, L.D. Knibbs, L. Morawska, Estimating the spatiotemporal variation of NO2 concentration using an adaptive neuro-fuzzy inference system, Environ. Model. Software 100 (Feb. 2018) 222–235, https://doi.org/10.1016/j.envsoft.2017.11.031.

[54] N.Ö. Doğan, Bland-Altman analysis: a paradigm to understand correlation and agreement, Turk J Emerg Med (Sep. 2018), https://doi.org/10.1016/j.tjem.2018.09.001.

[55] E.P. Emov, Informe de Calidad de Aire Cuenca 2021, 2022. https://ierse.uazuay.edu.ec/proyectos/links_doc_contaminantes/Informes-Calidad-Aire/Informe_Calidad_Aire_Cuenca_2021.pdf. (Accessed 3 February 2023).

[56] Ministerio del Ambiente, Inventario de Emisiones de contaminantes del aire para los cantones Esmeraldas, Ibarra, Santo Domingo, Manta, Portoviejo, Milagro, Riobamba, Ambato y Latacunga, Año Base 2010 (2012). Vol. III 09-119, Quito, Ecuador.

[57] J.L. Fleiss, The design and analysis of clinical experiments. The Design and Analysis of Clinical Experiments, Feb. 1999, https://doi.org/10.1002/9781118032923.

[58] J.A. Adame, I. Gutierrez-Alvarez, J.P. Bolivar, M. Yela, Ground-based and OMI-TROPOMI NO2 measurements at El Arenosillo observatory: unexpected upward trends, Environ. Pollut. 264 (Sep. 2020) 114771, https://doi.org/10.1016/j.envpol.2020.114771.

[59] I. Ialongo, H. Virta, H. Eskes, J. Hovila, J. Douros, Comparison of TROPOMI/Sentinel-5 Precursor NO& lt;sub& gt;2& lt;/sub& gt; observations with ground-based measurements in Helsinki, Atmos. Meas. Tech. 13 (1) (Jan. 2020) 205–218, https://doi.org/10.5194/amt-13-205-2020.

[60] U. Jeong, H. Hong, Comparison of total column and surface mixing ratio of carbon monoxide derived from the TROPOMI/Sentinel-5 precursor with in-situ measurements from extensive ground-based network over South Korea, Rem. Sens. 13 (19) (Oct. 2021) 3987, https://doi.org/10.3390/rs13193987.

[61] M.A. Zambrano-Monserrate, M.A. Ruano, Has air quality improved in Ecuador during the COVID-19 pandemic? A parametric analysis, Air Quality, Atmosphere and Health 13 (8) (2020) 929–938, https://doi.org/10.1007/S11869-020-00866-Y/TABLES/3.

[62] M. Cazorla, E. Herrera, E. Palomeque, N. Saud, What the COVID-19 lockdown revealed about photochemistry and ozone production in Quito, Ecuador, Atmos. Pollut. Res. 12 (1) (Jan. 2021) 124–133, https://doi.org/10.1016/J.APR.2020.08.028.
[63] H. Pacheco, S. Díaz-López, E. Jarre, H. Pacheco, W. Méndez, E. Zamora-Ledezma, NO2 levels after the COVID-19 lockdown in Ecuador: a trade-off between environment and human health, Urban Clim. 34 (2020) 100674, https://doi.org/10.1016/J.UCLIM.2020.100674.
[64] P. Sicard, et al., Amplified ozone pollution in cities during the COVID-19 lockdown, Sci. Total Environ. 735 (Sep. 2020) 139542, https://doi.org/10.1016/J.SCITOTENV.2020.139542.
[65] K. Anbari, Y.O. Khaniabadi, P. Sicard, H.R. Naqvi, R. Rashidi, Increased tropospheric ozone levels as a public health issue during COVID-19 lockdown and estimation the related pulmonary diseases, Atmos. Pollut. Res. 13 (12) (Dec. 2022) 101600, https://doi.org/10.1016/J.APR.2022.101600.
[66] C. Tudor, Ozone pollution in London and Edinburgh: spatiotemporal characteristics, trends, transport and the impact of COVID-19 control measures, Heliyon 8 (11) (Nov. 2022) e11384, https://doi.org/10.1016/J.HELIYON.2022.E11384.
[67] J. Qi, et al., An observation approach in evaluation of ozone production to precursor changes during the COVID-19 lockdown, Atmos. Environ. 262 (Oct) (2021), https://doi.org/10.1016/J.ATMOSENV.2021.118618.
[68] A. Tobías, et al., Changes in air quality during the lockdown in Barcelona (Spain) one month into the SARS-CoV-2 epidemic, Sci. Total Environ. 726 (Jul. 2020) 138540, https://doi.org/10.1016/J.SCITOTENV.2020.138540.
[69] S.L. Altshuler, T.D. Arcado, D.R. Lawson, Weekday vs. weekend ambient ozone concentrations: discussion and hypotheses with focus on Northern California, J. Air Waste Manage. Assoc. 45 (12) (1995) 967–972, https://doi.org/10.1080/10473289.1995.10467428.
[70] W.S. Cleveland, T.E. Graedel, B. Kleiner, J.L. Warner, Sunday and workday variations in photochemical air pollutants in New Jersey and New York, Science (1979) 186 (4168) (1974) 1037–1038, https://doi.org/10.1126/SCIENCE.186.4168.1037.